Available online at www.sciencedirect.com
ScienceDirect
Journal of Power Sources 165 (2007) 598–608
JOURNAL OF POWER SOURCES
www.elsevier.com/locate/jpowsour

Lithium-ion batteries based on carbon–silicon–graphite composite anodes

Volodymyr G. Khomenko [a], Viacheslav Z. Barsukov [a], Joseph E. Doninger [a,*], Igor V. Barsukov [b]

[a] *Kiev National University of Technologies & Design, 2, Nemirovich-Danchenko str., Kiev 02011, Ukraine*
[b] *Superior Graphite Co. 10 South Riverside Plaza, Suite 1470, Chicago, IL 60606, USA*

Available online 30 November 2006

Abstract

The paper is devoted to the development of lithium-ion battery grade negative electrode active materials with higher reversible capacity than that offered by conventional graphite. The authors report on results of their experiments as related to the electrochemical performance of silicon-based materials for lithium-ion batteries. A commercial grade of spherically shaped natural graphite (FormulaBT™ SLA1025) was modified in a number of different ways with nano-sized silicon. The reversible capacity of SLA1025 modified by 9.2 wt% of the nano-sized amorphous silicon was seen to be as high as 590 mAh g^{-1}. The irreversible capacity loss with this compound was 20%. Lithium-ion batteries using such material were observed to display sharp capacity decay during prolonged cycling. In contrast, the reversible capacity of another experimental grade, the SLA1025 modified by 7.9 wt% of the carbon-coated Si was as high as 604 mAh g^{-1}. The irreversible capacity loss with this material was as low as 8.1%. This grade, also, was seen to display much better cycling performance than the baseline natural graphite.

A series of full lithium-ion rechargeable cells were developed in the CR2016 coin cell configuration. Higher specific capacity of graphite modified by silicon was observed. This allowed decreasing graphite content in the lithium-ion cells by a factor of 1.6. The resultant lithium-ion batteries after optimization of their composition displayed approximately 20% higher gravimetric and volumetric specific energy densities than lithium-ion battery based on conventional natural graphite.

Keywords: Lithium-ion battery; Natural graphite; Silicon–carbon–graphite composite anodes; PUREBLACK® Carbon; Expanded graphite

1. Introduction

The advantages of the lithium-ion batteries (LIBs) over traditional battery chemistries have been widely recognized. A particular interest to the end-user appears to be lithium-ion chemistry's high energy density (in excess of 150 Wh kg^{-1}) [1].

Currently, lithium-ion technologies employ various forms of graphite and/or graphitized carbon as active materials of the negative electrodes. Attempts are being made to achieve in practicality [2,3], and then to further exceed graphite's specific capacity (whose theoretical value is 372 mAh g^{-1}) which would result in a "leap-frog" increase of the specific energy density of LIBs. Since their commercialization in 1991, much effort has been devoted to improve the performance of LIBs resulting in almost doubling the energy density of commercial cells (the volumetric energy density has increased from 250 to over 400 Wh l^{-1}) [4]. However, rapid development of portable electronic devices imposes a continuously growing demand for even lighter-weight and smaller-sized rechargeable batteries. The further improvement of LIBs would become possible when the application of new electrode materials with higher specific volumetric capacity is adopted.

Recently, various materials (such as Si, Sn, Al [5–8], metal oxides [9–11], hard carbons [3,12–14], etc.) capable of reversible lithium storage have been investigated for the purpose of increasing the specific capacity of the negative electrode as well as full batteries.

Thus, it is known that silicon can form alloys with lithium electrochemically, allowing a composition of up to 4.4 Li per Si, potentially yielding an extremely large theoretical specific capacity of 4200 mAh g^{-1} [15–17]. This value is significantly higher than the theoretical capacity of graphite. Therefore, it is not surprising that there has been a considerable interest recently in silicon based electrode materials. However, the limiting factor to commercializing such materials is the large volumetric changes that occur during the charge–discharge cycling of silicon [16–18]. Also, its low conductivity results in a high

* Corresponding author. Present address: Dontech Global, Inc., 427 East Deerpath Rd., Lake Forest, IL 60045, USA. Tel.: +1 224 436 4835; fax: +1 847 234 4835.
E-mail addresses: vkg@svitonline.com (V.G. Khomenko), chemi@mail.vtv.kiev.ua (V.Z. Barsukov), jdoninger@dontechglobal.com (J.E. Doninger), ibarsukov@superiorgraphite.com (I.V. Barsukov).

0378-7753/$ – see front matter © 2006 Elsevier B.V. All rights reserved.
doi:10.1016/j.jpowsour.2006.10.059

irreversible capacity loss (a difference between the charge and discharge capacity on the first few formation cycles).

Multiple attempts have been made recently to solve these problems. Much effort has been devoted to investigation of electrodes obtained by deposition of silicon-based films of different types onto the current collectors [19–24]. On the other hand, the capacity of a given cell size mostly depends on the active materials loading. The above-mentioned electrodes had a silicon thickness in the range from 100 Å up to a few μm. Taking into account the density (~2.3 g cm^{-3}) and the maximum capacity (4200 mAh g^{-1}) of silicon, the maximum specific capacity of such electrodes could be less than 1 mAh cm^{-2} (due to lower loading of active materials), which is several times lower than the specific capacity of commercial electrodes based on graphite (4–7 mAh cm^{-2}) [1].

Some research groups have taken a direction of modifying conventional anode active materials, and later reported some of these to be quite promising for application in practical batteries. Specifically, combinations of carbon, silicon and some additional elements (such as, for instance, Sn and Sb) capable of reversible reaction with lithium ions were reported as a way to increase the specific capacity of electrodes [25–36]. It was found that dispersing ultra fine silicon particles within graphite matrix and then coating the surfaces of Si particles provides an effective way to compensate noticeably for volumetric changes [37–40]. Some of these approaches have been applied, and then further successfully developed by Superior Graphite Co. (USA) for manufacturing of various silicon–carbon–graphite composite materials [41].

The goal of the present study was to assess the performance capability of such materials, as well as to estimate a possible practical effect for their application in electrochemical devices. In this study, the authors have focused on the application of two types of modified silicon-based natural graphite synthesized in the industrials facilities of Superior Graphite Co. Their electrochemical behavior is reported in the half cells, as well as for the first time in the full small-size lithium-ion rechargeable cells.

2. Experimental/materials and methods

2.1. Electrode materials

2.1.1. Anode materials

The performance of thermally purified natural crystalline flake graphite with high packing density, as well as that of its derivatives, was studied in this work. The materials were manufactured by Superior Graphite Co. (Chicago, IL, USA). Thus, the baseline negative electrode active material was prepared from natural crystalline flake graphite obtained via flotation of graphite concentrate and then purified by subjecting it to the uniform heat treatment at temperatures in excess of 2500 °C. Purified flake, in the subsequent stages of processing, was reduced in size by milling and classification technologies to the degree that the resultant product ended up with spheroidally shaped particles with a mean particle size of 20 μm and featuring increased packing density in excess of 0.85 g cm^{-3}. The FormulaBT™ SLA1025 grade was selected as a baseline for this investigation and the design of the lithium-ion battery. In this paper, this graphite is denoted as SLA1025.

Silicon-based graphite was developed by Superior Graphite Co. in cooperation with Kiev National University of Technologies and Design. In order to produce a successful sample, several silicon deposition technologies were investigated with the precursor graphite. The most efficient technology chosen, which resulted in the production of the desired nano-sized silicon deposit, was a reductive decomposition of a silicon precursor on the surface of graphite FormulaBT™ SLA1025. The performance of this graphite is reported in this paper with the sample being denoted as SLA1025/Si.

The second silicon-based graphite was prepared by coating SLA1025/Si with a poorly graphitic carbon coating using standard in-house particle surface coating technologies of Superior Graphite Co. [42]. In further references throughout the paper this sample is denoted as SLA1025/Si/C.

The silicon content in the final material was determined by the analyses of the ash content of graphite materials after oxidation in an oxygen atmosphere. This method is based on the assumption that the materials contained only Si and C. The calculation of the Si content was based on the change in weight during oxidation of graphite material when heated in the oxygen flow at 950 °C. The amount of Si was calculated in accordance with the following equation:

$$Si + O_2 = SiO_2 \quad (1)$$

The ash content for the SLA1025 was considered to be zero, because this value was negligible (less then 0.05 wt%). Thus, the samples of SLA1025/Si and SLA1025/Si/C contained 9.2 wt% and 7.9 wt% Si, respectively.

2.1.2. Cathode materials

In this work, a commercial grade of lithium cobalt oxide manufactured by LICO Technology Corporation (available through Pred Materials International, Inc., New York, NY, USA) was used. The commercial grade L210 was selected for investigation and design of the lithium-ion battery. L210 grade was synthesized from the battery grade chemicals Co_2O_3 and Li_2CO_3. This material has a narrow particle size distribution (D_{50} = 10–12 μm) and high tap density (2.7–2.95 g cm^{-3}). The material was designed for the high capacity lithium-ion battery.

Different percolating materials were investigated in order to prepare a high performance cathode. The following graphite–carbon materials have been tested as conductivity enhancement additives: thermally expanded graphite [43] ABG1015, ABG-74, ABG1005 (the later having mean particle size of 5 μm) and 200 nm size PUREBLACK®205-110 Carbon (a new material on the battery market, best described as nano-sized partially graphitized carbon black [44]). All of the conductive diluents listed above are commercial products of Superior Graphite Co. (USA). Experiments were also run with Pred Materials' graphite AB 065M (grade KS-6) and AB 222M (grade SFG-6) from TIMCAL Ltd. (Switzerland), and a carbon black (grade EO-1) from Dneprodzerzhinskii coke-chemical plant (Ukraine).

2.1.3. Negative and positive electrode preparation

The active materials were mixed with the amount of 7–9 wt% polyvinylidene fluoride (PVDF) in *N*-methylpyrrolidine (NMP) solution. The mixture was agitated by using a high shear mixer. The resulting slurry was cast onto a metal foil (0.015 mm thick Al in the case of positive electrodes, and Cu in the case of negative electrodes), and a doctor blade with a gap opening of 254 μm was used to define the maximum thickness of the freshly coated layer. The resulting film was dried at 120 °C under the air flow, in order to evaporate the NMP. The electrodes were compacted to the desired density by means of calendaring. After compaction, the electrodes were dried again under a primary vacuum at 120 °C in the time frame of 12 h. The active loading of the anode and cathode was in the range of 6–12 and 15–30 mg cm^{-2}, respectively. The thickness of the electrodes was monitored with a Mitutoyo (Japan) micrometer. The thicknesses of the electrodes were in the range 0.06–0.10 mm. The average density of graphite layer was in the range of 1.4–1.6 g cm^{-3}. The average density of cathode layer was kept in the range 2.3–3.2 g cm^{-3}.

2.2. Materials characterization

The SLA1025 grade and Si-modified graphite samples as received have been characterized by X-ray. The silicon powder (99.8 wt% purity) was ball milled in a specialized chamber under Ar atmosphere using carbide tungsten balls. Then Si powder was pounded with a mortar and pestle to break apart agglomerated particles before X-ray characterization.

X-ray diffraction analysis of the powder was conducted in a Philips X'pert X-ray diffractometer using Cu Kα radiation.

The microstructures of these materials were examined using a transmission electron microscope (CM 20 Philips) and a scanning electron microscope JEOL JSM-6320F.

2.3. Electrochemical characterization

The disc electrodes having a diameter of 16 mm were cut out of the coated film cast onto metal foil current collector using a punch. The coin cells (CR2016 standard size) were assembled in a glove box filled with argon (Unilab model, MBraun, USA). The following procedure was employed: (i) the electrode was placed in the bottom can; (ii) ∼19.5 mm diameter separator TEKLON™ EDEX separator (manufactured by ENTEK Membranes LLC, USA) was placed on the face of the electrode and affixed to it by a polypropylene o-ring gasket, (iii) the electrolyte (1 M $LiPF_6$ in a 1:1 volume mixture of ethylene carbonate (EC) and dimethyl carbonate (DMC) provided by MERCK, Germany) was spread on top of the separator; (iv) the nickel grid (∼14 mm diameter) was welded to the top cap of the cell. After that, a 16 mm diameter Li disk was placed on the Ni grid of the cap. In the case of a mockup of a full lithium-ion cell, the Ni spring was placed in the cap of the cell (the spring was not used in the case of the "half-cells", where a Li foil counter electrode was used); (v) the coin cell was compressed and sealed using a coin-cell crimping device.

Galvanostatic charge/discharge cycling was performed using a 32-channel automatic battery tester and battery cycler (MSTAT 32 from Arbin Instruments, USA).

3. Results and discussion

3.1. Physico-chemical characterization

3.1.1. XRD investigation

The X-ray diffraction patterns of the SLA1025, Si based graphites and that of pure Si are shown by Fig. 1. In accordance with the X-ray characterization, different crystalline structures of Si were defined for the SLA1025/Si and SLA1025/Si/C composite materials. The SLA1025/Si samples mostly contained Si in the amorphous form, which is expected to occur due to the high-temperature decomposition of the Si precursor. The SLA1025/Si/C contained crystalline Si. The diffraction peaks of the Si and the SLA1025/Si/C samples were similar to the key diffraction peaks, typical for powdered crystalline Si (noteworthy is the lower intensity of the characteristic peak in the SLA1025/Si/C sample due to the low content of Si in this sample). It should be mentioned that all graphite samples containing Si resulted in no change in the crystalline structure of the graphite. The diffraction peak (0 0 2) is seen to be well defined for all graphite grades. This suggests that the deposit of Si on the graphite is similar to a coating, rather than to a doping on a molecular level.

3.1.2. SEM investigation

Fig. 2 reveals scanning electron microscope images of the materials under investigation. Thus, a photomicrograph referring to Fig. 2(a) depicts a spheroidal morphology and the rounded-edge particles of the baseline natural graphite SLA1025 with a mean particle size of approximately 20 μm.

The general appearance of the SLA1025/Si composite is given in Fig. 2(b). An analysis of this figure shows that: (i)

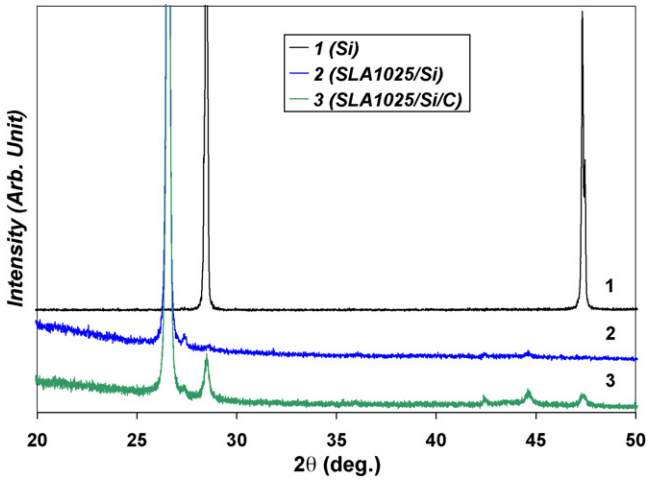

Fig. 1. XRD pattern of: (1) silicon powder; (2) as-received natural graphite modified by 9.2 wt% nano-particles of silicon (sample SLA1025/Si); (3) as-received natural graphite modified by 7.9 wt% carbon-coated silicon-natural graphite composite (sample SLA1025/Si/C).

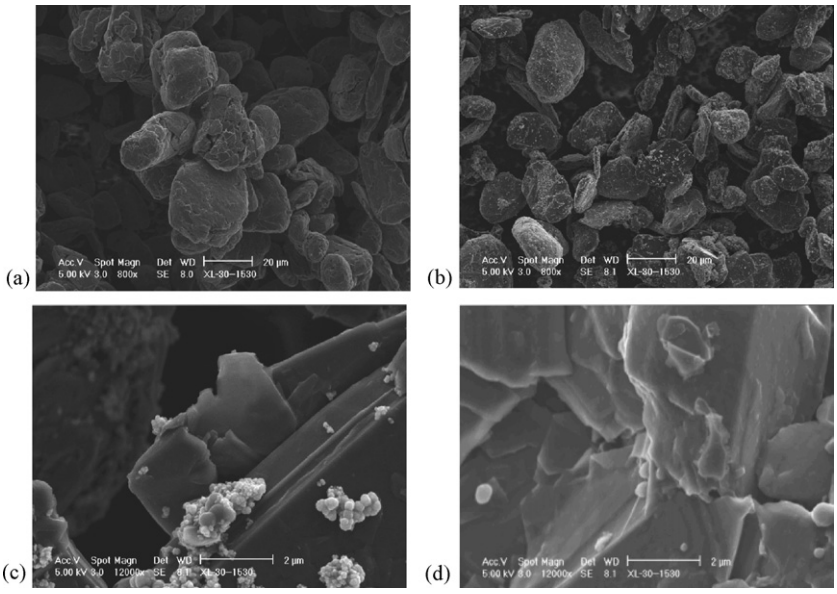

Fig. 2. Scanning electron microscope images of purified rounded-edge natural crystalline flake graphite SLA1025 (a); silicon-coated natural graphite SLA1025/Si at different magnifications (b and c); carbon–silicon-natural graphite composite SLA1025/Si/C (d).

Si was decomposed on graphite in the form of nano-particles, which formed a coating, rather than acting as a dopant, thus supporting an earlier conclusion from the XRD tests (Fig. 1) on the nature of SLA1025/Si compound; (ii) silicon was deposited onto the bulk graphite quite uniformly.

Fig. 2(c) depicts a fragment of SLA1025/Si compound at a higher magnification than what is shown by Fig. 2(b) (12,000× versus 800×, respectively). From Fig. 2(c), the size of the silicon deposit can generally be estimated, which is in the range of 50–1000 nm. Despite macro-scale uniformity evident from Fig. 2(b), it can be seen that on a micro level, particles of silicon were lumped together—a typical result, which can be confirmed by the crystal growth theory for uncompleted metal coatings.

The SEM of a typical fragment of the SLA1025/Si/C composite can be seen in Fig. 2(d). A comparison of the appearance of materials given in Fig. 2(c and d) at similar magnification (12,000×) suggests that the stabilizing carbon coating uniformly covered both the flake core and the silicon particles on the surface. It is further seen that during the process of application of stabilization carbon coating, the silicon agglomerates depicted in Fig. 2(c) were broken down and individual crystals of silicon were smeared onto the surface of graphite, while some "excess" silicon appears to have been knocked out from the SLA1025 core and lost (a parallel evidence for this observed in the previously reported experiments on determining the concentration of Si in SLA1025/Si and SLA1025/Si/C).

3.1.3. TEM investigation

The microstructure of SLA1025/Si and SLA1025/Si/C composites was examined using transmission electron microscopy (TEM) combined with selected area diffraction. The TEM micrographs of Si nano-particles in the SLA1025/Si sample are shown by Fig. 3. The silicon particles appear to be shaped as balls (many of which are sized at less than 100 nm diameter), and form long aggregates. The selected area diffraction pattern (see insert in Fig. 3) does not exhibit a clear ring pattern, indicating the amorphous nature of Si particles. The TEM of the carbon-coated silicon–graphite composite (which is identified as SLA1025/Si/C) is shown by Fig. 4. The selected area diffraction pattern (see insert in Fig. 4) exhibits a partial ring pattern, indicating the nano-crystalline nature of Si within the amorphous carbon matrix. The change from the amorphous nature of Si in SLA1025/Si versus partially crystalline nature of Si in SLA1025/Si/C sample is explained by the authors as a result of a high temperature heat-treatment (in excess of 1000 °C), which the sample was subjected to during the process of stabilization of the carbon coating on SLA1025/Si/C material. The presence of the dark field on the TEM image of the carbon-coated silicon nano-composite suggests that Si particles have shrunk to sizes

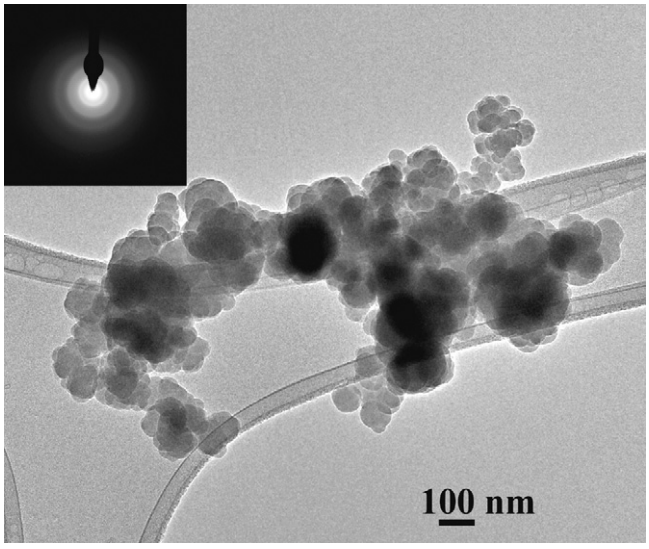

Fig. 3. TEM micrographs of Si nano-particles on the surface of composite SLA1025/Si.

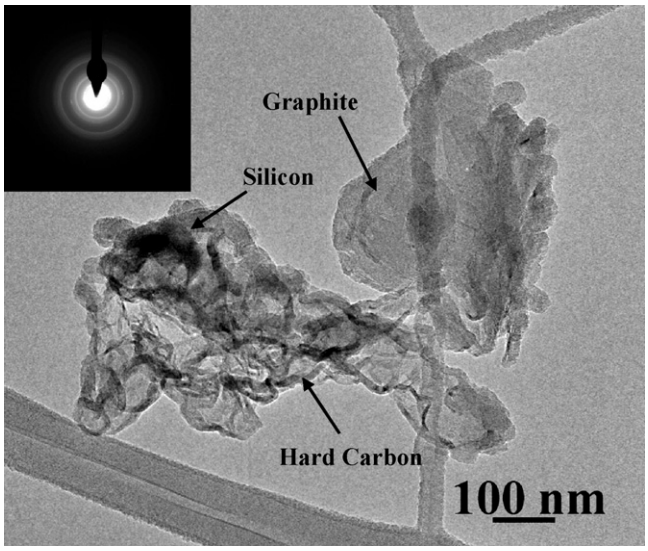

Fig. 4. TEM micrographs of carbon coated silicon-natural graphite composite (sample SLA1025/Si/C).

of less than 50 nm, and became more irregular as compared with the amorphous silicon, which was distributed on the precursor carbon, SLA1025/Si.

3.2. Electrochemical characterization

3.2.1. Electrochemical performance of SLA1025 graphite

In the present work, the performance of as-received and silicon modified SLA1025 graphite grades in the electrodes of lithium-ion batteries were evaluated.

Fig. 5 shows voltage profiles of the as-received graphite at different current densities (the values are reported in the C-rates). The experiment was conducted in the CR2016 coin cells with a Li metal counter electrode. On the first charge (intercalation), the potential drops rapidly after slight retardation at approximately 0.8 V. The main intercalation and deintercalation of lithium takes place at potentials of lower than 0.3 V versus Li/Li$^+$ reference electrode and is accompanied by three potential plateaus. The initial capacity of SLA1025 on deintercalation of Li$^+$ was seen to be $Q_1 = 352\ \text{mAh g}^{-1}$ at the current density of $25\ \text{mA g}^{-1}$ ($\sim C/15$) within the range of cut-off potentials of 0.01 and 1.5 V. The capacity consumed upon the first charge is not fully recovered upon the following discharge. The capacity that cannot be recovered is called the "irreversible capacity loss" and is observed at the first charge/discharge cycles. Irreversible capacity was $\Delta_1 = 8.5\%$. At the second and subsequent cycles, graphite SLA1025 shows a good reversibility with a Coulombic efficiency of ~100%. The reversible specific capacity depends on the current rate applied. With the increase of the current density from $C/15$ to C, the capacity of SLA1025 decreased from 352 to $158\ \text{mAh g}^{-1}$. On the other hand, the capacity of SLA125 was still quite high ($267\ \text{mAh g}^{-1}$) at the current density of $70\ \text{mA g}^{-1}$ ($\sim C/5$). The typical voltage profile of Li deintercalation was still evident at high current rate. Thus, it should be noted that the decrease of capacity may also be related to the polarization of Li counter electrode, which could not be reversibly charged/discharged at high current density.

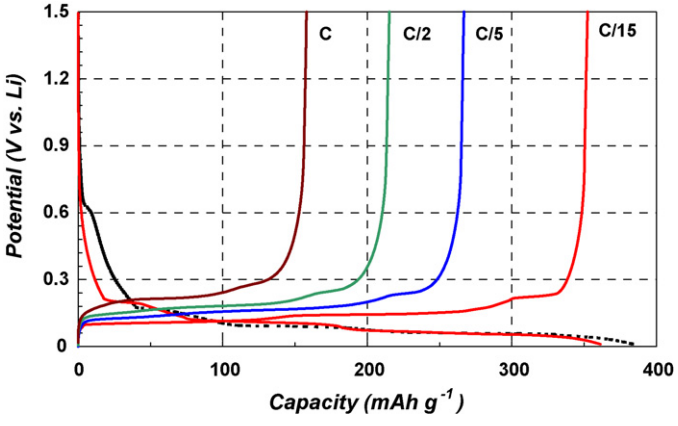

Fig. 5. Profiles of charge/discharge potentials of the round-edge purified natural graphite (grade SLA1025) at different current density (the discharge profiles at $C/5$, $C/2$ and C are not shown). Please note the difference between the first discharge (dotted line) at $C/15$ and the second cycle, which is due to formation of the SEI.

The above-mentioned hypothesis has been validated in a tree-electrode electrochemical cell of a T-cell configuration. By design, all three electrodes in this cell were lithium. Fig. 6 represents a typical current–potential curve for determining polarization resistance. It should be mentioned that the current density at 1 C rate for electrodes with active loading of graphite in the range of 6–12 mg cm^{-2} lead to a current density of about 2–4 mA cm^{-2} per surface area of Li electrode. The polarization of Li electrode at such current density could be in the range 0.2–0.4 V according to Fig. 6. Thus, high polarization of Li electrode could not allow the intercalation of Li into graphite at the appropriate range of potentials.

The curves in Fig. 7 depict prolonged cycling performance of SLA1025-based electrode at a current density rate of $25\ \text{mA g}^{-1}$ ($\sim C/15$). It can be seen that the capacity of SLA1025 was quite stable during the cycling. It should be noted that graphite SLA1025 was able to efficiently work at electrode densities of about $1.6\ \text{g cm}^{-3}$, allowing for up to 25% improvement of the electrode energy density in comparison with that for a non-spherical graphite.

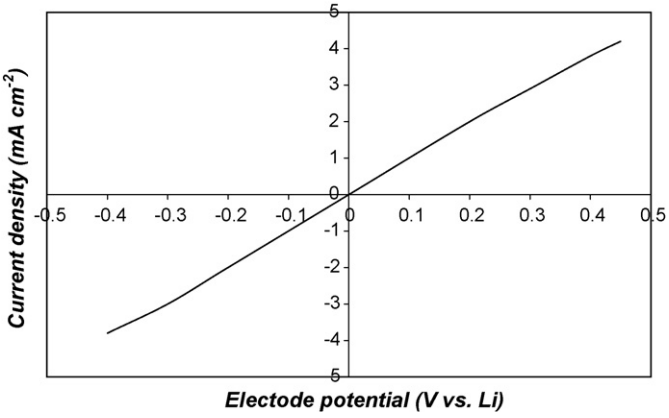

Fig. 6. Current density as a function of electrode potential of Li electrode in the 1 M $LiPF_6$ in EC/DMC.

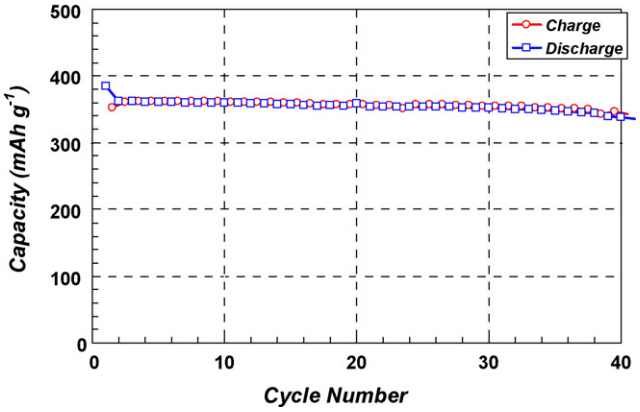

Fig. 7. Specific capacity vs. cycle number for the round-edge purified natural graphite (grade SLA1025). Capacities were obtained at ~C/15 (25 mA g^{-1}) rate. The cut-off potentials were 1.5 V for charge and 0.01 V for discharge.

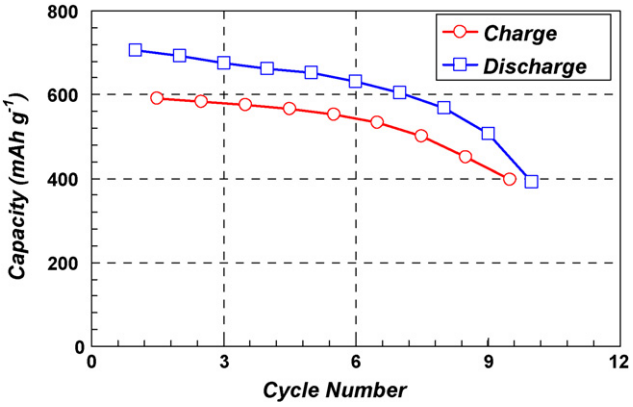

Fig. 9. Specific capacity vs. cycle number for graphite modified by 9.2 wt% nano-sized particles of silicon (SLA1025/Si grade). Capacities were obtained with a current density 30 mA g^{-1}. The cut-off potentials were 1.5 V for charge and 0.01 V for discharge.

3.2.2. Electrochemical performance of SLA1025/Si composite

Fig. 8 shows voltage profiles of SLA1025 modified by 9.2 wt% of Si (denoted as SLA1025/Si) at the current density of 30 mA g^{-1}. At the first intercalation and deintercalation, the capacity of SLA1025/Si composite was 705 mAh g^{-1} and ~590 mAh g^{-1}, respectively. The irreversible capacity loss was 20%, which is quite high for applications in practical lithium-ion batteries. Taking into account the capacity of SLA1025 determined in the previous experiments, the capacity of Si (Q_{Si}) can be expressed as (2):

$$Q_{Si} = \frac{(Q_{SLA1025/Si} - Q_{SLA1025} \times C_{SLA1025})}{C_{Si}} \quad (2)$$

where $Q_{SLA1025/Si}$ is the specific capacity of SLA1025/Si; $Q_{SLA1025}$ the specific capacity of graphite SLA1025; $C_{SLA1025}$ the weight fraction of graphite SLA1025; and C_{Si} is a weight fraction of silicon in the composite material SLA1025/Si.

The calculation using Eq. (2) gives a capacity value of approximately 3910 mAh g^{-1} for the first alloying reaction between lithium and Si (upon first intercalation), and 2960 mAh g^{-1} for the first reaction upon deintercalation. These data show that alloy

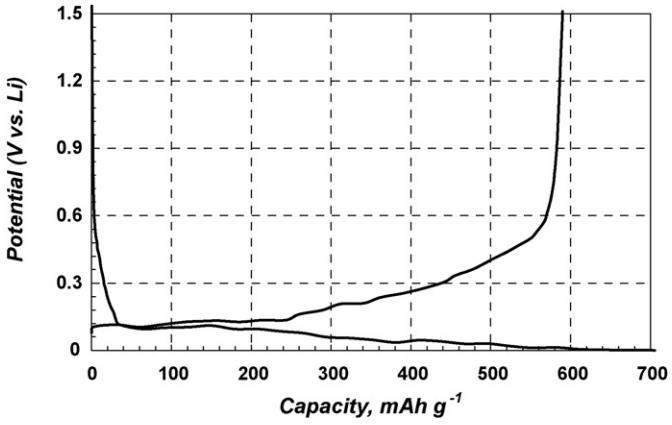

Fig. 8. Profiles of the charge/discharge potentials of the natural graphite modified by 9.2 wt% nano-sized silicon (SLA1025/Si grade) at current density of 30 mA g^{-1}.

like $Li_{3.5}Si$ or higher content of Li could be formed during intercalation of Li into Si. In the papers [15,45], the authors reported the possibility of the formation of such alloys at low temperature. The obtained data agrees closely with the specific capacity of amorphous Si reported by Jung et al. [20].

Fig. 9 shows how the specific capacity versus cycle number changes for SLA1025/Si. The cycling was performed at a constant current of 30 mA g^{-1}. Unfortunately, electrodes of such type show sharp capacity decay during the cycling. The mechanism of this fading should be investigated in more depth in the future. The simple volumetric expansion of amorphous Si [9] is, most likely, one, but not the only factor responsible for the rapid capacity fade. This is due to the fact that Si was obtained in the form of nano-particles, which were well dispersed in the bulk graphite material. Some ideas about the reasons for C/Si composite capacity fade were expressed in the work by Dimov et al. [45,46]. The authors speculate over an idea that electrodes based on Si may be loosing the contact between the current collector and the active layer. Thus, improved cycling performance was observed in the case of a three-dimensional current collector (for example, Ni foam) [27]. In our tests, we have also established that after cycling, the graphite layer has had virtually no adhesion with the copper foil, while particle-to-particle cohesion was near perfect. In other words, the graphite layer, which lost contact with copper foil was quite homogeneous with any other deformation of the graphite films not being evident. Therefore, we suggest that loss of adhesion of the active layer to the current collector leads to capacity fade. Further investigation of this hypothesis continues. The easiest way to optimize the electrode was to encapsulate the graphite coated with silicon with an amorphous coating and at the same time a hard carbon coating—an approach discussed in the next section.

3.2.3. Electrochemical performance of SLA1025/Si/C composite

The SLA1025/Si composite was further optimized by applying the rigid carbon coating as an outer shell around each Si-coated particle of graphite. Carbon coating is now a standard technique, which Superior Graphite applies to its advanced

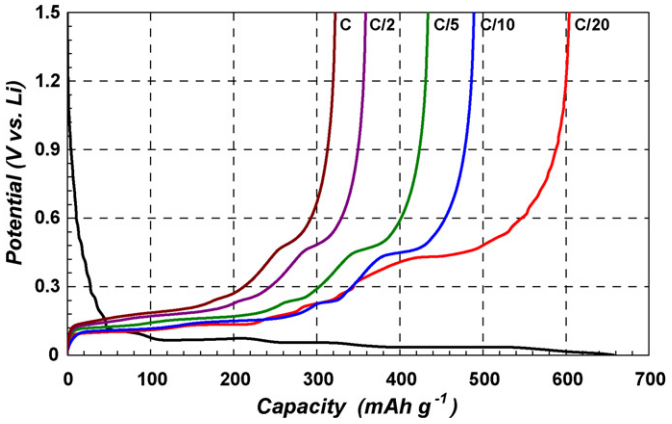

Fig. 10. Profiles of the charge/discharge potentials of the carbon coated silicon–graphite composite (SLA1025/Si/C grade) cycled at different current densities (the discharge profiles at *C*/10, *C*/5, *C*/2, *C* are not shown).

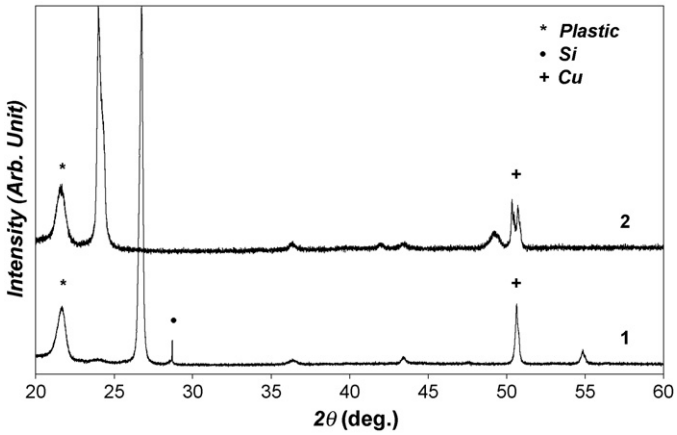

Fig. 11. XRD pattern before (curve 1) and after (curve 2) intercalation of electrode, based on natural graphite modified by 7.9 wt% carbon-coated silicon-natural graphite composite (SLA1025/Si/C grade).

lithium-ion battery grades of graphite. Its nature and properties have been discussed earlier [42,49]. Results of our experiments have shown this optimization to be a promising approach, which can significantly improve the properties of the Si-based composite materials. Additionally, the authors of [46,47] also report a much better cycling performance with their carbon coated silicon and other Si-based materials.

There are two effects of carbon coating: (i) the carbon coating should be diminishing the expansion of Si particles; (ii) the carbon coating is believed to be partially suppressing the reaction of Si particles with lithium ions. The later may subsequently be leading to the formation of dense blocks and clusters, which are unable to take part in the electrochemical processes.

Fig. 10 shows the voltage profiles of the SLA1025/Si/C composite grade at different current densities. Such types of materials are characterized by the presence of a large potential plateau in the range of potentials from 0.3 to 0.5 V in their deintercalation profiles. It appears that that the high capacity increase with this material is caused by Li alloying reaction with silicon nano-particles. At the first intercalation and deintercalation reactions, the SLA1025/Si/C composite demonstrated capacity values of 657 and 604 mAh g^{-1}, respectively. The irreversible capacity loss of as low as 8.1% has been observed with this material, which is a promising value for the practical application in full lithium-ion batteries [1]. To the best of our knowledge, this is the first time that such a low irreversible capacity of Si-based materials is being reported in the literature. As one can judge from the comparison of Figs. 5 and 10, graphite SLA1025/Si/C has shown higher capacity than pure graphite (SLA1025) by approximately a factor of 1.6.

With the increase of the current density from *C*/20 to *C*, the capacity of SLA1025/Si/C composite decreased from 604 to 322 mAh g^{-1} while the capacity of SLA1025/Si/C was still very high (434 mAh g^{-1}) at a current density of 80 mA g^{-1} (∼*C*/5 rate). This observation resulted in conclusion that the Si-based compounds can also be intercalated/deintercalated quickly. A typical voltage plateau at about 0.4 V, which is related with delithiation of Si, was presented on all curves obtained at the high current density. It should be noted that capacity of Si-based anodes was higher than that for the anodes based on graphite SLA1025 at all current densities studied. The decrease of capacity at the high rate may also be explained by the limitations of the testing device, in that the high polarization of Li counter electrode may have played a role in preventing the intercalation of Li at the appropriate range of potentials.

Calculation using Eq. (2) gives a capacity value of approximately 3840 mAh g^{-1} for the first alloying reaction between lithium and Si (upon the first intercalation), and 3410 mAh g^{-1} for the first de-alloying reaction at a current density of 30 mA g^{-1}. These data suggests that alloys of an approximate composition of $Li_{3.5}Si$ or even the alloys with higher content of Li could be formed during the reaction between Li and Si.

An XRD investigation of electrode based on SLA1025/Si/C has been conducted in order to determine the crystallographic nature of the alloy. Fig. 11 compared the X-ray difractograms of the electrode before (curve 1) and after (curve 2) intercalation. Starting from fully delithiated graphite with 0 0 2 peak at around 26.6° (d_{002} = 3.35 Å) the peak shifted to the lower angle. After full lithiation at 0 V versus Li in graphite the 0 0 1 peak typical for of stage 1 was seen to be at 24.2° (e.g. d_{001} = 3.71 Å), as presented by the X-ray diffraction pattern (curve 2). However, there are no new considerable peaks, which deal with Si alloy formation. Probably the electrochemically formed alloy of Si leads to formation of compounds which are partly or completely amorphous. Similar conclusion was drawn in Refs. [50,51] where Li^+ insertion in the silicon was studied in detail using various techniques.

Fig. 12 shows a long-term cycling performance of SLA1025/Si/C-based electrode at the current density of 30 mA g^{-1}. It depicts much better cycling performance than the composite of SLA1025/Si. Thus, the carbon coating has improved, and the capacity stability of Si particles was reached, probably, due to enhancement of the binding strength between the particles of graphite and silicon. Further studies are needed to clarify the capacity fading mechanism, which is still taking place with the composite material in question.

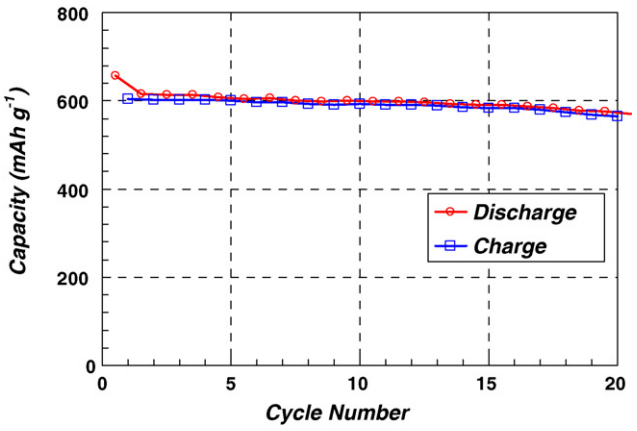

Fig. 12. Specific capacity vs. cycle number of the carbon coated silicon–graphite composite (sample SLA1025/Si/C). Capacities were obtained at current density of 30 mA g^{-1}. The cut-off potentials were 1.5 V for charge and 0.01 V for discharge.

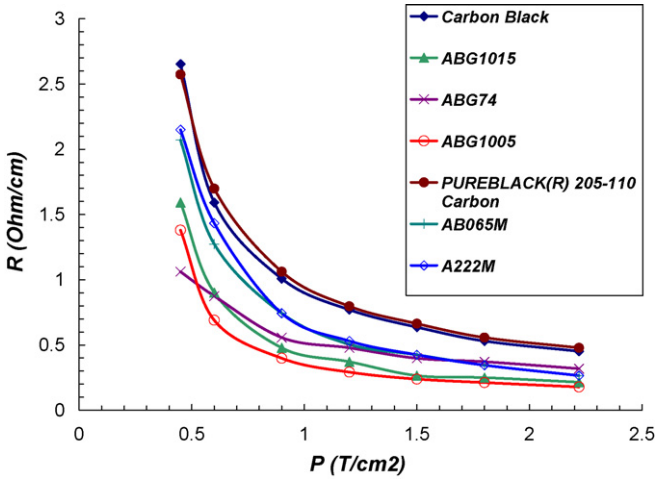

Fig. 13. The resistance (R) of active mass depending on pressure (P) of formation of samples based on MnO_2 (85 wt%) as a function of carbon diluent (10 wt%). The balance of electrode composition is made up by 5 wt% PVDF binder.

3.2.4. Electrochemical characterization of the cathode

The KNUTD has developed a set of unique laboratory equipment for the four-point measurement of the electrical resistance of active materials, which can be compacted to pellets or rings at a pressure up to 3 metric tonnes per square centimeter. The four-point measurement method is very accurate and reliable, as it diminishes the possibility of errors due to possible poor contacts and polarization effects. The above-mentioned equipment allows optimizing the content of the active materials versus the content of conductive diluents and other additives in the electrodes. It has been used in our design work with the high-energy density batteries, as reported below.

In order to select the best conductivity enhancement additive for $LiCoO_2$ matrix, initially authors carried out the measurements of conductivity of the cathode masses based on MnO_2 (the size of particle was in the same range as that for $LiCoO_2$). The electrodes also contained 10 wt% carbon materials and 5 wt% PVDF. The MnO_2 was chosen in order to avoid the loss of environmentally unfriendly $LiCoO_2$ (for each measurement the device uses approximately 5 g of metal oxide). Fig. 13 shows the resistance of active mass depending on pressure and type of carbon diluents used.

Tests have shown that the lowest resistance is demonstrated by a cathode mass based on the expanded graphite (ABG1005, ABG74, ABG1015 grades). The lowest resistance of all the materials tested was seen for an electrode composition based on the expanded graphite ABG1005. These graphitic materials were selected for the development of electrode.

The electrochemical properties of $LiCoO_2$ electrode were examined using the CR2016 coin-type half-cells with Li-foil counter electrode. The charge/discharge behaviour of the cathode was evaluated in the course of galvanostatic cycling at the different current rates within the potential range of 2.5–4.2 V. The electrochemical investigations have shown that highly compacted electrodes based on ABG1005 alone, used as conductive additive, demonstrate low capacity and high polarization. It seems that applying a high compaction pressure during the calendaring of the expanded graphite between the rolls diminishes the electrode porosity and therefore the electrolyte content in the bulk of the electrode. The carbon black and a new form of conductive additive on the battery market, known as PUREBLACK® Carbon (commercial product of Superior Graphite Co., USA [48]) were seen to be good at complementing performance of expanded graphite in the cathodes. These materials are good at adsorbing electrolyte and were seen to improve the mobility of Li^+ within the electrode.

The improvement of performance of power sources by application of the PUREBLACK® Carbon have been shown in Refs. [44,48]. The PUREBLACK® Carbon, being an ultra pure partially graphitized carbon black with properties exceeding those of battery grade acetylene blacks have higher conductivity than carbon black and feature higher packing density. Thus, the application of PUREBLACK® Carbon is preferable.

Electrodes with different contents of expanded graphite and PUREBLACK® Carbon were developed. The composition of electrodes versus capacity of $LiCoO_2$ at different current rates is summarized in Table 1. The highest capacity of $LiCoO_2$ at the high current density was obtained from electrodes based on the mixture of PUREBLACK® Carbon and expanded graphite added in the ratio of 1:3. Fig. 14 shows the discharge curves for the electrode, based on the selected optimum composition at different current rates. The discharge capacity of $LiCoO_2$ at

Table 1
Electrode compositions vs. capacity of $LiCoO_2$ at different current rates

Content of conductive additives in the cathode (%)		Current rate			
ABG 1005	PUREBLACK® 205–110 Carbon	*C*/10	*C*/5	*C*/2	*C*
100	–	121	109	87	58
–	100	141	126	112	82
30	70	140	135	123	113
50	50	138	131	111	92
70	30	139	134	132	130

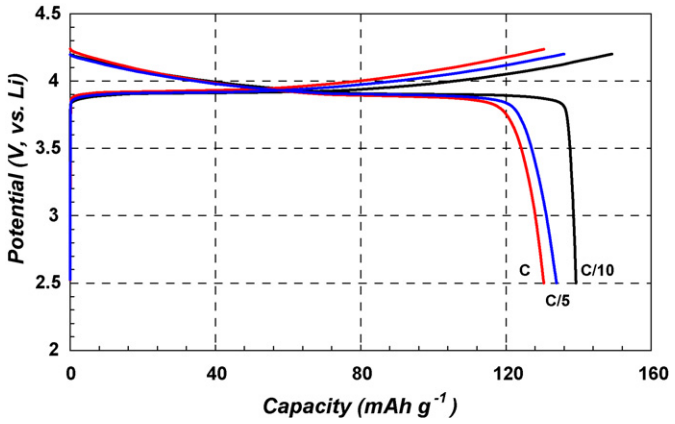

Fig. 14. Profiles of charge/discharge potentials of the cathode based on $LiCoO_2$ at different current densities.

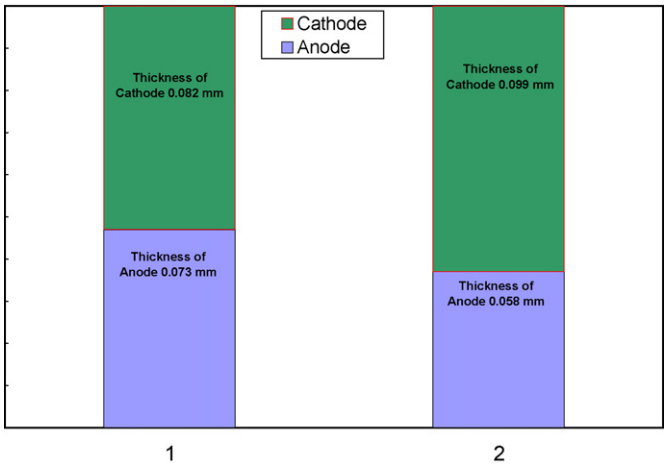

Fig. 15. The thickness of electrodes and corresponding volume fraction of electrodes in the coin cells based on graphite SLA1025 (1) and SLA1025/Si/C composite (2) anodes.

$\sim C/10$ was seen to be 139 mAh g^{-1}, while it was 130 mAh g^{-1} at the high rate ($\sim C$).

3.2.5. *Design parameters and electrochemical performance in the full lithium-ion cells*

Electrochemical performance of the silicon–carbon-based composite anodes was also assessed in the full cells. This is one of the first published reports by the authors on the full lithium-ion cell performance.

A critical design parameter of the full lithium-ion cells became a need to properly balance the overall capacity of $LiCoO_2$-based cathode with the practical output capacity of the graphite and/or silicon–carbon composite anode. In this case, the higher capacity capability of the anode made it possible to make it thinner, and accordingly, make up for the free in-cell volume with a thicker cathode.

It should be noted that if a lithium-ion cell were to be designed as being cathode limited, the deficit of $LiCoO_2$ in it would quickly lead to a decrease in capacity of such a cell. On the contrary, the excess of $LiCoO_2$ could lead to decrease of the operating cell voltage because the charge and discharge of graphite at the counter electrode would be occurring in a too narrow of a range of potentials. Too heavy loading of the cathode active could additionally lead to such an undesirable side reaction, as lithium metal deposition onto the anode during the charge process. In the case of metallic lithium plating on the electrode surface, it will be reacting with the electrolyte and may initiate a thermal runaway reaction in the cell [2].

Thus, the actual capacity ratio of the cathode to anode became an optimum based on a trade-off between the desire for higher capacity in the cells and the need for a safety factor to be engineered into the cell design. Specifically, the optimum cell balance was found to be with the mass ratio between $LiCoO_2$ and graphite modified by silicon as 3.9, and 2.3 for the non-modified graphite-containing cells, respectively.

A series of full lithium-ion rechargeable cells were developed in the CR2016 coin cell configuration. The lithium-ion coin cell was designed with a constant total thickness of electrodes in order to evaluate the effect of negative electrode active material modification by Si-based composites. The thickness of electrodes and corresponding volume fractions are shown on the diagram represented by Fig. 15. The higher specific capacity of the graphite modified by silicon allows for decreasing the graphite content in the lithium-ion battery by a factor of 1.6. Therefore, the fraction of the capacity of the positive electrode was increased in order to compensate for the freed-up volume in the cells. The coin cell based on SLA1025/Si/C composite anode had noticeably higher discharge capacity (6.8 mAh) than the cell based on baseline SLA1025 graphite anode (5.6 mAh).

Figs. 16 and 17 demonstrate typical voltage profiles of lithium-ion cells based on SLA1025 and SLA1025/Si/C, respectively. The capacity of these cells is only slightly decreased with the increase of the current density from $C/10$ to C rate. Thus, both of types of cells can be charged/discharged at "high" (practical) current rates.

The electrochemical characteristics of full cells are summarized in Table 2. The data presented is initial discharge values. For reference, the cell based on silicon–graphite composite (SLA1025/Si/C) was built from a 136 mAh g^{-1} $LiCoO_2$ cathode

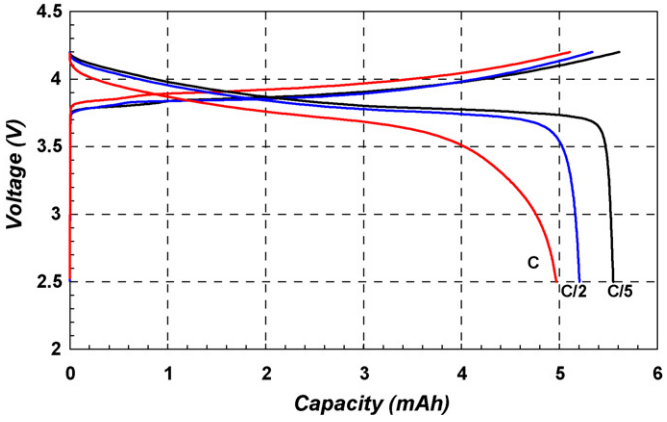

Fig. 16. Profiles of the charge/discharge voltage for the full rechargeable lithium-ion coin cell using the anode based on natural graphite (grade SLA1025). The cut-off voltages were 4.2 V for charge and 2.5 V for discharge. The capacity rates were $C/5$, $C/2$ and C.

Table 2
Characteristics of rechargeable lithium-ion coin cells as a function of graphite type used in the anode composition

Grade of graphite	U (V)	Capacity of cell (mAh)	Q_{LiCoO_2} (mAh g^{-1})	$Q_{graphite}$ (mAh g^{-1})	Energy density	
					Wh kg^{-1} [a]	Wh l^{-1}
SLA1025	4.2	5.6	132	304	168	588
SLA1025/Si/C	4.2	6.8	136	531	200	714

[a] The weight of 2016 cell enclosure is not considered.

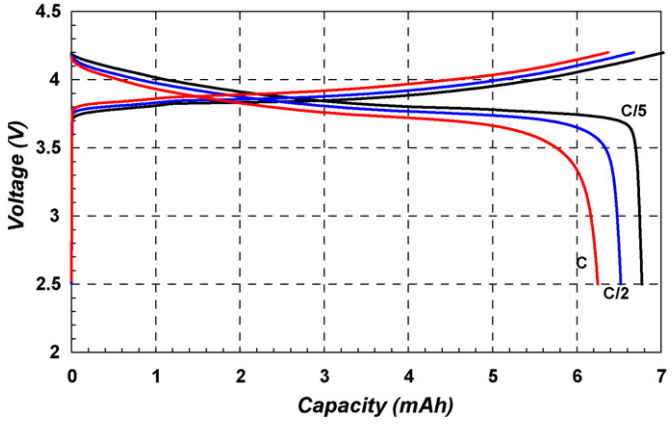

Fig. 17. Profiles of the charge/discharge voltage for the full rechargeable lithium-ion coin cell using the anode based on carbon coated silicon–graphite composite (sample SLA1025/Si/C). The cut-off voltages were 4.2 V for charge and 2.5 V for discharge. The capacity rates were *C*/5, *C*/2 and *C*.

and a 531 mAh g^{-1} composite graphite anode. In the reported values of the gravimetric energy density, the weight of the cell enclosure was not included as it is a function of the cell size and would have added unnecessary error if it were included.

An analysis of the data presented, results in a conclusion that full lithium-ion cells based on graphite–silicon composite anodes display approximately 20% higher gravimetric and volumetric specific energy densities than those for the cells based on baseline natural graphite anodes.

To the best of our knowledge, this is the first time that the performance advantages of the Si–graphite based composite materials was reported in the full cell configuration, which is very close to the practical lithium-ion battery. Achieving this result was possible due to the low irreversible capacity loss of the SLA1025/Si/C material, and also as a result of the focused effort on optimization of cathode to anode ratio with these new materials.

4. Conclusions

Modifications of graphite by silicon appears to be a promising approach to increasing the specific capacity of both the negative electrodes and that of the full lithium-ion batteries. The best results were achieved with composite materials based on thermally purified natural graphite first coated with 7.9 wt% nano-sized silicon and then enclosed into the hard shell of an amorphous carbon coating. Such materials were engineered and manufactured by Superior Graphite Co. (USA), and are referred to in the paper as SLA1025/Si/C composites.

The cathode to anode ratio of the full lithium-ion cells needs to be optimized in order to capitalize on the benefits of application of the higher capacity anodes. In an optimized cell configuration, we have seen an approximately 20% higher gravimetric and volumetric specific energy densities when a 360 mAh g^{-1} natural graphite (SLA1025) negative electrode active material was substituted with a 531 mAh g^{-1} silicon–graphite composite SLA1025/Si/C.

Stabilization carbon coating of the silicon–graphite composite resulted in a low irreversible capacity material (approximately 80 mAh g^{-1} (8.1%)), whose stability upon prolonged cycling has been dramatically improved over the cycling stability performance characteristics of the uncoated Si–graphite composite, studied by us and also by other authors. The mechanism of capacity fading with certain silicon–graphite composites cannot be simplistically explained by volumetric changes of silicon during its alloying reaction with lithium ions, and will be studied in more depth in the future.

An attempt to find the optimum conductive diluents for the $LiCoO_2$ cathode was also made. The best performing conductivity enhancement matrix for the cathodes studied was found to be a combination of 5 μm expanded graphite (ABG1005) with a new material on the battery market: a 200 nm, partially graphitized carbon black, known as PUREBLACK® 205–110 Carbon. The highest capacity of $LiCoO_2$ cathodes at the high current density has been obtained from electrodes based on the mixture of PUREBLACK® Carbon with expanded graphite, taken in the ratio of 1:3.

Future focus by the battery community on the proposed new materials and concepts appears to represent a viable new direction, which may result in creation of the next generation lithium-ion battery technologies featuring significantly improved energy density outputs.

Acknowledgements

Authors would like to thank Thomas Cacciaguerra (CRMD, CNRS University, Orleans, France) for developing high-resolution TEM images presented by Figs. 3 and 4. Two of the authors (VK and VB) acknowledge financial support by the Initiatives for Proliferation Prevention (IPP) project P-154, which is part of the non-proliferation program of the U.S. Department of Energy/National Nuclear Security Administration (DOE/NNSA). In addition, authors VK and VB wish to acknowledge the U.S. Civilian Research and Development Foundation, CRDF (Arlington, VA, USA), whose First Steps to Market program through grant number UE2-5006-KV-03 partially supported engineering and built of the 4-point resis-

tivity tester used to develop data reported in Fig. 13. The team of authors acknowledges assistance by Mr. Anatoliy Rolik of TechnoElectrochim Co. in Kiev, Ukraine, who contributed immensely to engineering and constructing of said devise. Authors VB and JD are grateful to the NATO Science for Peace program's project SfP 973849, entitled: "Carbons as Materials for the Electrochemical Storage of Energy", which brought together the U.S. and Ukraine teams, headed by them at the time.

References

[1] D. Linden, T.B. Reddy, Handbook of Batteries, third ed., McGraw Hill, New York, 2001.
[2] F. Cao, I.V. Barsukov, H.J. Bang, P. Zaleski, J. Prakash, J. Electrochem. Soc. 147 (10) (2000) 3579–3583.
[3] I.V. Barsukov, F.B. Henry, J.E. Doninger, P.L. Zaleski, M.A. Gallego, T. Huerta, G. Uribe, R. Girkant, D. Darwin, ITE Lett. Batteries New Technol. Med. 4 (2) (2003) 163–166.
[4] W. Schalkwijk, B. Scrosati (Eds.), Advances in Lthium-Ion Batteries, Kluwer Academic/Plenum Publishers, New York, 2002.
[5] M. Winter, J.O. Besenhard, Electrochim. Acta 45 (1999) 31.
[6] M. Inaba, T. Uno, A. Tasaka, J. Power Sources 146 (2005) 473–477.
[7] C. Arbizzani, S. Beninati, M. Lazzari, M. Mastragostino, J. Power Sources 161 (2006) 826–830.
[8] J. Yang, Y. Takeda, N. Imanishi, O. Yamamoto, J. Electrochem. Soc. 147 (2000) 1671.
[9] V.Z. Barsukov, J.E. Doninger, in: I.V. Barsukov, et al. (Eds.), New Carbon Based Materials for Electrochemical Energy Storage Systems: Batteries, Supercapacitors and Fuel Cells, Springer, The Netherlands, 2006, pp. 297–307.
[10] J. Yang, Y. Takeda, N. Imanishi, C. Capiglia, J.Y. Xie, O. Yamamoto, Solid State Ionics 152–153 (2002) 125–129.
[11] R. Alcántara, P. Lavela, G.F. Ortiz, J.L. Tirado, R. Stoyanova, E. Zhecheva, C. Merino, Carbon 42 (2004) 2153–2161.
[12] E. Buiel, J.R. Dahn, Electrochim. Acta 45 (1999) 121–130.
[13] E. Peled, V. Eshkenazi, Y. Rosenberg, J. Power Sources 76 (1998) 153–158.
[14] Y. Ohzawa, Y. Yamanaka, K. Naga, T. Nakajima, J. Power Sources 146 (2005) 125–128.
[15] P. Limthongkul, Y.-I. Jang, N.J. Dudney, Y.-M. Chiang, Acta Mater. 51 (2003) 1103–1113.
[16] J. Yang, M. Winter, J.O. Besenhard, Solid State Ionics 90 (1996) 281.
[17] R.A. Huggins, J. Power Sources 81–82 (1999) 13.
[18] J.O. Besenhard, J. Yang, M. Winter, J. Power Sources 68 (1997) 296.
[19] H.-C. Shin, J.A. Corno, J.L. Gole, M. Liu, J. Power Sources 139 (2005) 314–320.
[20] H. Jung, M. Park, Y.-G. Yoon, G.-B. Kim, S.-K. Joo, J. Power Sources 115 (2003) 346–351.
[21] M. Uehara, J. Suzuki, K. Tamura, K. Sekine, T. Takamura, J. Power Sources 146 (2005) 441–444.
[22] T. Takamura, M. Uehara, J. Suzuki, K. Sekine, K. Tamura, J. Power Sources 158 (2006) 1401–1404.
[23] T. Moon, C. Kim, B. Park, J. Power Sources 155 (2006) 391–394.
[24] Y.O. Illin, V.Z. Barsukov, V.S. Tverdokhleb, in: I.V. Barsukov, et al. (Eds.), New Carbon Based Materials for Electrochemical Energy Storage Systems: Batteries, Supercapacitors and Fuel Cells, Springer, The Netherlands, 2006, pp. 309–316.
[25] I.-S. Kim, P.N. Kumta, J. Power Sources 136 (2004) 145–149.
[26] M. Holzapfel, H. Buga, W. Scheifele, P. Novak, F.-M. Petrat, Chem. Commun. (2005) 1566–1568.
[27] M. Yoshio, T. Tsumura, N. Dimov, J. Power Sources 146 (2005) 10–14.
[28] M. Yoshio, S. Kugino, N. Dimov, J. Power Sources 153 (2006) 375–379.
[29] K. Hanai, Y. Liu, N. Imanishi, A. Hirano, M. Matsumura, T. Ichikawa, Y. Takeda, J. Power Sources 146 (2005) 156–160.
[30] D. Larcher, C. Mudalige, A.E. George, V. Porter, M. Gharghouri, J.R. Dahn, Solid State Ionics 122 (1999) 71–83.
[31] Y. Liu, K. Hanai, J. Yang, N. Imanishi, A. Hirano, Y. Takeda, Solid State Ionics 168 (2004) 61–68.
[32] N. Dimov, S. Kugino, M. Yoshio, J. Power Sources 136 (2004) 108–114.
[33] A. Netz, R.A. Huggins, W. Weppner, J. Power Sources 119–121 (2003) 95–100.
[34] Y. Liu, K. Hanai, K. Horikawa, N. Imanishi, A. Hirano, Y. Takeda, Mater. Chem. Phys. 89 (2005) 80–84.
[35] N. Dimov, H. Noguchi, M. Yoshio, J. Power Sources 156 (2006) 567–573.
[36] X.-W. Zhang, P.K. Patil, C. Wang, A.J. Appleby, F.E. Little, D.L. Cocke, J. Power Sources 125 (2004) 206–213.
[37] N. Dimov, K. Fukuda, T. Umeno, S. Kugino, M. Yoshio, J. Power Sources 114 (2003) 88–95.
[38] N. Dimov, S. Kugino, M. Yoshio, Electrochim. Acta 48 (2003) 1579–1587.
[39] H. Li, X. Huang, L. Chen, Z. Wu, Y. Liang, Electrochem. Solid State Lett. 2 (1999) 547–549.
[40] I. Kim, P. Kumta, G.E. Blomgren, Electrochem. Solid State Lett. 3 (2000) 493–496.
[41] J.S. Gnanaraj, M.K. Gulbinska, J.F. DiCarlo, I.V. Barsukov, N. Holt, V.Z. Barsukov, J.E. Doninger, in: I.V. Barsukov, et al. (Eds.), New Carbon Based Materials for Electrochemical Energy Storage Systems: Batteries, Supercapacitors and Fuel Cells, Springer, The Netherlands, 2006, pp. 317–331.
[42] F.-X. Henry, I.V. Barsukov, J.E. Doninger, S. Anderson, P.R. Booth, P.L. Zaleski, R.J. Girkant, D.J. Derwin, M.A. Gallego, T. Huerta, G. Uribe, in: I.V. Barsukov, et al. (Eds.), New Carbon Based Materials for Electrochemical Energy Storage Systems: Batteries, Supercapacitors and Fuel Cells, Springer, The Netherlands, 2006, pp. 213–229.
[43] I. Barsukov, J. Doninger, P. Zaleski, D. Derwin, ITE Lett. Batteries New Technol. Med. 2 (1) (2000) 106–110.
[44] I. Barsukov, Ind. Miner. 8 (2004) 75.
[45] N. Dimov, S. Kugino, M. Yoshio, Electrochim. Acta 48 (2003) 1579–1587.
[46] N. Dimov, K. Fukuda, T. Umeno, S. Kugino, M. Yoshio, J. Power Sources 114 (2003) 88–95.
[47] T. Umeno, K. Fukuda, H. Wang, N. Dimov, T. Iwao, M. Yoshio, Chem. Lett. (2001), CL-010828.
[48] I.V. Barsukov, M.A. Gallego, J.E. Doninger, J. Power Sources 153 (2006) 288–299.
[49] J. Liu, D.R. Vissers, K. Amine, I.V. Barsukov, J.E. Doninger, in: I.V. Barsukov, et al. (Eds.), New Carbon Based Materials for Electrochemical Energy Storage Systems: Batteries, Supercapacitors and Fuel Cells, Springer, The Netherlands, 2006, pp. 283–292.
[50] P. Limthongkul, Young-Il Jang, N.J. Dudney, Yet-Ming Chiang, Acta Mater. 51 (2003) 1103–1113.
[51] J. Li, Solid State Ionics 135 (2000) 181–191.